Dearborn, Michigan
NOISE-CON 2008
2008 July 28-30

Sound radiated by a resonant plate: comparative evaluation of experimental and computational methods

Murat Inalpolat[a]
Gear Dynamics and Gear Noise Research Laboratory, The Ohio State University
Columbus, Ohio 43210, USA

Mehmet Caliskan[b]
Department of Mechanical Engineering, Middle East Technical University
06531 Ankara, Turkey

Rajendra Singh[c]
Acoustics and Dynamics Laboratory, The Ohio State University
Columbus, Ohio 43210, USA

ABSTRACT

Near field radiation behavior of a free-free, lightly damped square plate, which is excited at its midpoint, is analytically and experimentally studied. First, the plate is computationally discretized into equal segments that are replaced by simple, phase-correlated acoustic sources. Piston radiator models (with and without mutual radiation impedance terms) are examined along with the pulsating sphere model. The radiated power from phase-correlated discrete sources is calculated; their individual phases are obtained from the surface vibration measurements. Second, the two-microphone acoustic intensity and the surface intensity techniques are employed to determine the radiated sound power on both narrow and 1/3 octave band bases up to 1600 Hz covering radiation from several vibration modes. Finally, an indirect boundary element model is used to predict the sound power spectra, as well as to simulate the two-microphone method given surface vibration data. All predictions are compared with measurements. Discrepancies between theory and experiments (and even between two intensity measurements) are discussed along with possible sources of error.

1. INTRODUCTION

Near field radiation information is often needed to quantify relatively noisy regions on the vibrating surfaces, radiation paths, and acoustic "short-circuiting" [1]. In particular, this could be helpful in understanding the radiation mechanism of thin, lightly damped resonant plates, which are typically found in machinery casings[2, 3]. Since the near fields of resonant plates with classical boundaries have been studied by only a few researchers[4-7] a thin, lightly damped square plate (with free boundaries) is chosen as the example in our study. Such structures are routinely examined in industry via modal testing as well as pressure to force type frequency response function measurements under freely suspended conditions[8-10]. Since a closed form solution for sound power for this particular structure is not available, we will apply analytical, computational and experimental methods. Our analytical models (discretized sources) would examine the role

[a] Email address: inalpolat.1@osu.edu
[b] Email address: caliskan@metu.edu.tr
[c] Email address: singh.3@osu.edu

of both self and mutual impedance terms. Further, an indirect boundary element formulation (BEM) is used to predict sound power as well to assess possible experimental errors. The main focus is not to validate any models, but rather to comparatively evaluate the methods and to demonstrate their applicability to a problem of significant interest from machinery noise reduction perspective. On a more fundamental basis, we also pose an interesting (and perhaps even a benchmark) problem for researchers and practitioners.

2. PROBLEM FORMULATION

The scope of the investigation is limited by the following: 1. A thin square plate ($300\,mm \times 300\,mm \times 1\,mm$) is chosen as the example since elastic plates are found in many engineering applications. The example case is shown in Figure 1; the free-free plate is excited by a point force at its midpoint ($x = 0, z = 0$). 2. No baffle is intentionally considered in our study to simulate industrial test conditions. 3. Both narrow band (particularly at resonant frequencies) and 1/3 octave-band spectra of sound power up to 1600 Hz are considered. 4. Given the near field location, the Helmholtz number is less than 0.55 at 1600 Hz. Table 1 lists five models that are employed to predict sound power. Three discrete acoustic radiation models[11-15] are employed to predict the near field radiation. Two simple models (*A1 and B*) do not incorporate any acoustic interactions, but *Model A2* does and it is expected to reveal the influence of mutual interactions on near field radiation. Further explanation of these models will be given in section 3. Experiments are carried out to assess the applicability of discrete radiation models. Both two-microphone acoustic intensity (I_m) and surface intensity (I_s) measurement techniques are applied to determine the radiated sound power (W) from the top surface of the plate, as shown in Figure 1. However, the measured narrow band spectra from these two techniques are not very close. To examine the underlying reasons, discrete radiation models are re-examined along with two models (*C1 and C2*) based on the indirect boundary element method. BEM models are also used to predict the near field effects. Main objectives of this study are thus to: (a) Explore the applicability of discrete sound radiation models as well as conventional intensity measurement methods to relatively complex acoustic sources exhibited by the example case, (b) Comparatively evaluate analytical, computational and experimental methods in terms of sound radiated by resonant modes up to 1600 Hz.

Table 1: Overview of analytical and computational methods employed.

Model Number	Model Type	Mutual Interactions	Brief Description
Model A1	Baffled-piston radiator	Excluded	Intended more for far field estimations
Model A2	Baffled-piston radiator	Included	Intended more for near field estimations
Model B	Pulsating sphere	Excluded	Expected to give rough estimations
Model C1	Indirect BEM	Included	Generates comparable results to discrete models
Model C2	I_m simulation by BEM	Included	To check near field radiation and errors in modeling

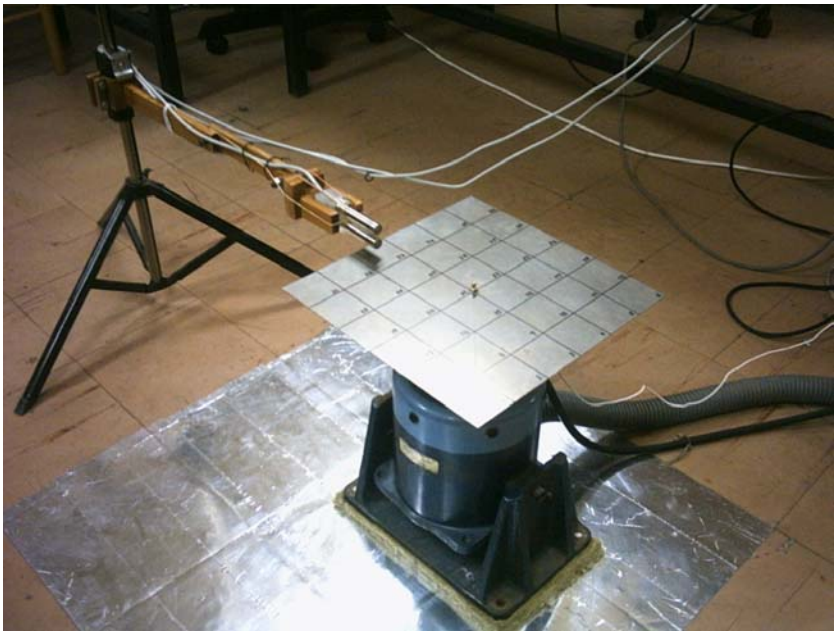

Figure 1: Example case (free-free steel plate) and near-field acoustic intensity (I_m) measurements.

3. NEAR FIELD PREDICTIONS BY SIMPLE DISCRETE RADIATOR MODELS

Discrete models are widely used to model acoustic radiation from relatively simple structures; for example, refer to the book[15] by Koopman and Fahnline that includes many examples. However, the authors calculate radiation from either idealized or "controlled" sources. In our study, three different radiation models are used to predict the near field radiation from a resonant plate with phase-correlated and interacting sources. First, two different versions of a vibrating piston source model (*A1* and *A2*) are used to understand the influence of acoustic mutual interaction terms. Second, a pulsating sphere formulation (*B*) (without any mutual interactions) is used to roughly evaluate the vibrating piston models.

A. Discrete Piston Radiator Sources and the Effect of Mutual Interactions

The plate is discretized into segments as shown in Figure 2. Then a vibrating circular piston (assumed to be in an infinite baffle) is placed at the center of each segment. *Model A1* includes the phase relations among the vibrating segments and the relative phase spectra are obtained via vibration measurements at 36 discrete points ($\Delta x_S = \Delta z_S = 0.05\, m$). Note that *Model A1* excludes the mutual radiation impedance effects[16, 17] and therefore it is expected to yield a rough estimate of the near field. In *Model A1*, each segment of area S_i is virtually replaced by a circular vibrating piston (of radius a_i such that $S_i = \pi a_i^2$) radiating with its own phase. Here, the subscript i refers to the i^{th} discrete element (segment) on the plate. The reason for using 36 partitions is that the I_m measurements showed that an increase in the number of partitions beyond 36 did not considerably improve the W spectrum. Expression for W for the i^{th} piston is given by

$$W_i = 0.5\pi a_i^2 U_i^2 \rho_o c_o R_{ii}\left(\Gamma\right), \tag{1}$$

where $\Gamma = 2ka_i$, U is surface velocity (measured) and R_{ii} is self-radiation resistance in force to velocity units[16]. The near field pressure distribution ($P(\kappa)$, where j is the imaginary unit and κ is an arbitrary point on the radiating piston) is given as follows[17]:

$$P(\kappa) = \left(\left(jk\rho_o c_o U_i \right) / 2\pi \right) \int_{-\pi/2}^{\pi/2} d\theta \int_{0}^{2r_1\cos(\theta)} \left(e^{-jkR} / R \right) RdR \quad . \tag{2}$$

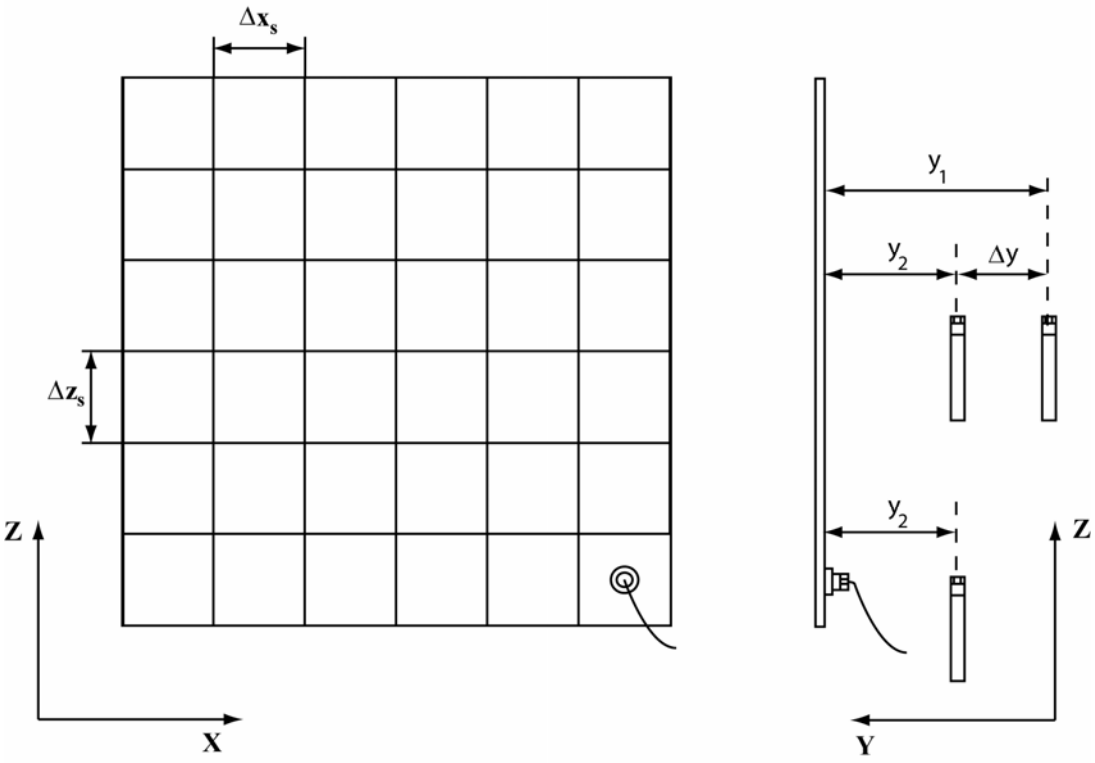

Figure 2: Schematic of the plate (including discretized elements) and intensity measurements (both surface and 2-microphone methods), in the Cartesian coordinate system. Microphones in the near field along with an accelerometer on the surface are shown.

Two infinitesimal elements are arbitrarily chosen on the surface of the piston where d is the differential element. One of these areas (dS_1) is exactly at point κ and the other ($dS_2 = R\,dR\,d\theta$) is at point δ, which is at distance R and angle θ with respect to point κ. Here, $dS_1 = r_1\,dr_1\,d\tau$ where r_1 is the distance (radius) from point κ to the center of the piston, and τ is the polar angle of point κ with respect to the center of the piston. The limits of the second integral are the points at both ends of the vector connecting the points (κ and δ). Note also that dS_2 is already written explicitly in the free field Green's Function (e^{-jkR}/R) in the above integration. The total force exerted by the sound field on the piston is given by $F_i = \int P(\kappa) dS_1$ [16, 17]. The self-radiation impedance, $Z_{ii} = F_i / U_i$, is then found as,

$$Z_{ii} = \rho_o c_o S_i \left[1 - \left(\frac{2J_1(\Gamma)}{\Gamma} \right) + j \left(\frac{2H_1(\Gamma)}{\Gamma} \right) \right]. \quad (3)$$

Here, J_1 is the Bessel function (first order), H_1 is the Struve function (first order). The total sound power is finally found by a superposition of the results from 36 sources. Then, since the mutual radiation in the near field is of importance, *Model A2* is formulated next, where the mutual interaction effects (with d_{ij} as the distance between the i^{th} and j^{th} pistons) are represented by the following mutual impedance (Z_{ij}) terms[17].

$$Z_{ij} = \left(\left(\rho_o c_o k^2 S_i S_j \right) / 2\pi \right) \left[\left(4J_1(\Gamma/2) \right) / \Gamma \right]^2 \left(\left(\sin\left(kd_{ij} \right) / kd_{ij} \right) + j \left(\cos\left(kd_{ij} \right) / kd_{ij} \right) \right). \quad (4)$$

The sound power radiated by the i^{th} piston radiator (with both self and the mutual radiation impedances) is calculated as follows where **Re** is the real part of the complex valued expression:

$$W_i = \mathrm{Re}\left(Z_{ii} \right) \left| U_i \right|^2 + \sum_j \mathrm{Re}\left(Z_{ij} U_i U_j^* \right). \quad (5)$$

Then, total W is found by a superposition of the W_i terms. In our study, Struve Function is approximated by the following simplified expression[18] where $\beta = 1/\pi$, and J_0 is the Bessel function (zeroth order). This expression reduces the computational time and programming effort.

$$H_1\left(\Gamma\right) = (2\beta) - J_0\left(\Gamma\right) + ((16\beta) - 5)(\sin\left(\Gamma\right)/\Gamma) + (12 - (36\beta))(1 - \cos\left(\Gamma\right)/(\Gamma)^2). \quad (6)$$

B. Discrete Pulsating Sphere Sources (Without Mutual Interactions)

The pulsating sphere formulation (*Model B*) is employed next to estimate sound power and to assess other models. Like *Model A1*, *Model B* is also expected to give a rough estimation because it excludes the mutual radiation effects. The total power (W) from the plate is then found by summing the powers radiated by 36 phase-correlated segments, each radiating W_m that is given by the following based on a pulsating sphere (of radius a_m) formulation that is restricted to half-space :

$$W_m(\omega) = (\pi \rho_o {U_m}^2 {a_m}^4 \omega^2) / (c_o \left(1 + \left(\Gamma/2 \right)^2 \right)). \quad (7)$$

4. NEAR FIELD ACOUSTIC AND SURFACE INTENSITY MEASUREMENTS

The experimental set-up (Figure 1) consists of sound intensity and surface intensity probes, two accelerometers with signal conditioners and two dynamic signal analyzers. An electro-dynamic shaker excites the plate through band-limited random or swept sine signals that are fed to the shaker by means of a power amplifier and a two-channel dynamic signal analyzer. The sound intensity probe was designed to hold two transducers (such as 12.5 *mm* phase-matched B&K

4165 condenser microphones) at an arbitrary angle; an effort was made to minimize the coefficient of reflection. Note also that the laboratory floor is wrapped with an aluminum sheet to maximize reflection of the sound waves from the floor, as shown in Figure 1. The sound intensity I_m spectrum, at frequency ω (rad/s), is determined by using the well-known two-microphone expression[19]:

$$I_m(\omega) = (1/\omega\rho_o\Delta y)\,\mathrm{Im}\left(G_{P_2P_1}(\omega)\right). \tag{8}$$

Here, G is the cross power spectrum, P_2 and P_1 are the complex-valued pressure amplitudes at y_2 (closer to the measurement surface) and y_1 (at Δy from y_2) respectively, and ρ_o is the air density (1.205 kg/m^3 at the room conditions); 64 ensemble averages are taken at each measurement point. The side-by-side probe configuration (as shown in Figures 1 and 2) is utilized for sound intensity measurements in the y direction (normal to the plate) with a separation of $\Delta y = 18$ mm in a plexiglass holder with a special arrangement that maintains Δy between the microphones. Acoustical center of the microphone (P_2) closer to the plate is at $y = 8$ mm from the surface of the plate. Sound pressure and sound intensity calibrators are employed for the calibration of measurement microphones. Finally, the sound power spectrum (W) is calculated and expressed in dB re 1 pW, both in narrow and 1/3 octave band forms.

The microphone at y_2 is used together with an accelerometer placed onto the plate to measure the surface intensity I_s, as schematically shown in Figure 2. It is expressed by

$$I_s(\omega) = (-1/\omega)\,\mathrm{Im}\left(G_{AP_2}(\omega)\right), \tag{9}$$

where $G_{AP_2}(\omega)$ is the single-sided cross spectrum between the acceleration (A) and the pressure P_2 signals; 64 averages are taken for each spectral measurement. A low mass accelerometer (2.5 $grams$) is used to reduce the mass loading effect. The I_s data is taken at 36 grid points of the plate like the I_m measurement. All of the surface intensity (I_s) measurements are made on a grid with 36 partitions. Finally, both I_s and I_m spectra are post-processed via Matlab routines.

Concurrent with I_m and I_s measurements, the surface vibration data is recorded at 36 discrete (grid) points on the plate to determine the surface velocity amplitude U_i, averaged mean-square velocity $\langle \psi_u^2 \rangle_s$, and operational deflection shapes of the plate. Figure 3 shows the measured sound power (W) spectra via I_m and I_s techniques on a narrow band basis up to 1600 Hz; also, $\langle \psi_u^2 \rangle_s$ spectrum is plotted. Note that a reference of 10^{-6} m/s is chosen for the surface velocity level so that its spectral shape (in dB) could be compared with the W spectra ($re\,1\,pW$) obtained by I_m or I_s measurements. Observe that the W with I_s technique closely follows the $\langle \psi_u^2 \rangle_s$ spectrum, unlike the results with I_m.

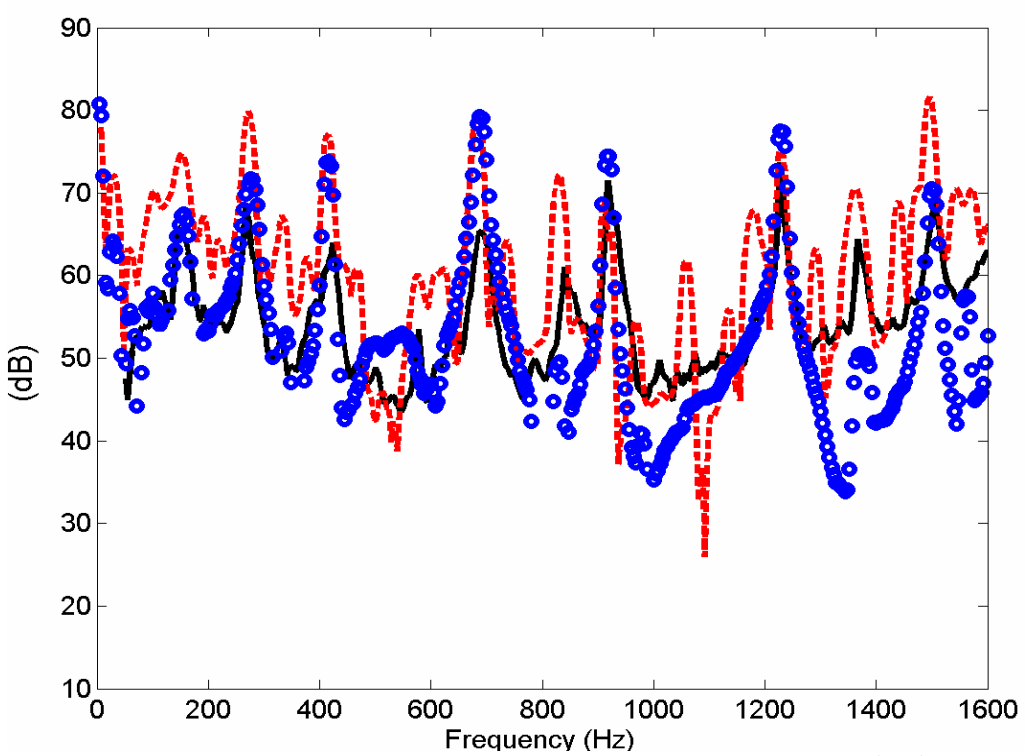

Figure 3: Measured sound power (W, dB re 1.0 pW) and mean-square surface velocity ($\langle \psi_u^2 \rangle_s$, dB re 10^{-6} m/s), on a narrow band basis. Key: Red dotted line (---): W by the surface intensity (I_s) method; blue circles (o o o) W by the two-microphone acoustic intensity (I_m) method; black solid line (—): measured mean-square velocity $\langle \psi_u^2 \rangle_s$.

To further examine the power spectra, radiation efficiency (σ_{rad}) levels ($dB\, re\, 1$) are calculated using $W = \sigma_{rad} \rho_o c_o S_a \langle \psi_u^2 \rangle_s$, where S_a is the total radiation area, c_o is the speed of sound in air, and σ_{rad} is the radiation efficiency. The radiation efficiency spectra exhibit a pattern similar to that of the sound power spectra and thus not reported here. Although discrepancies exist at some frequencies, results are relatively close, mostly at the peaks (plate resonant frequencies). Yet, it is also observed that I_m based results yield a smoother spectrum with fewer sharp peaks. This might be due to a sharp gradient of the acoustic particle velocity (U_p) with distance y away from the surface where as the structural velocity (U_i) is measured by the I_s method. Other sources of error will be discussed in section 6.

5. NEAR FIELD PREDICTIONS BY THE BOUNDARY ELEMENT METHOD

An indirect boundary element formulation (*Model C1*) is also employed to calculate W directly by an implicit routine[20]. The solution to the Helmholtz Equation is expressed in terms of surface potentials ($\tilde{\Phi}(x, y, z)$). A variational approach is then used to solve the integral equations that relate the unknowns, single layer (of density $\sigma_s(\tilde{p})$) monopole type sources and double layer (of density $\sigma_d(\tilde{p})$) dipole type sources $\sigma_s(\tilde{p})$ and $\sigma_d(\tilde{p})$ on S to the applicable boundaries.

Gunda and Vijayakar[21] have discussed details of the fast multi-pole formulation and its computational efficiency. In our study, the structural dynamics of the plate is first analyzed using a finite element model with 144 elements. Then, this structural model along with the mesh is imported into the boundary element software. Surface velocity amplitudes (U_i) gathered via accelerometers are imposed (in *Model C1*) as velocity boundaries. Further, an analysis is carried out to ensure whether the number of elements used in the structural finite element model is sufficient for predicting the near-field pressures. To accomplish this, the power radiated by the plate is directly found by the built-in sound power routine of the boundary element software[20]. Next, the same boundary element method is then utilized to simulate two pressures at y_1 and y_2 (as shown in Figure 2), and estimate the W spectrum like the two-microphone acoustic intensity (I_m) experiment (as described in section 4). This particular model is designated as *Model C2*. The aim is to see if any near field measurement errors could be identified. In our work, pressures P_1 and P_2 are estimated at y_2 and y_1 (like the I_m measurements), with $\Delta y = 18\,mm$, and $y = 17\,mm$ (distance from plate to the acoustic center of microphones as shown in Figure 2). The particle velocity (U_p) is estimated by calculating the single-sided cross power spectrum as $G_{P_2P_1}(\omega) = P_2^*(\omega)P_1(\omega)$, instead of using the finite difference formula. Acoustic intensity (I_m) spectrum is then calculated by using equation (9).

6. COMPARATIVE RESULTS AND SOURCES OF ERROR

Results from 5 models and 2 experiments are compared in Table 2 and Figure 3. First, we examine the sound power levels (in Table 2) at resonant frequencies of the plate since they dominate the spectra as seen in Figure 3. Further, natural frequencies of this plate are calculated by using the finite element method, and the following resonant frequencies are close (within 5%) to the measured ones: 247 Hz, 411 Hz, 676 Hz, 919 Hz, 1218 Hz, and 1486 Hz. Many more modes (including repeated roots given the symmetric nature) are of course obtained in the analysis but only certain modes (as mentioned above) are excited. As shown in Figure 3, the narrow band sound power spectra are dictated by resonances and anti-resonances of the plate. In order to have a greater clarity in the comparisons and to emphasize the role played by resonances (dominant sources), sound powers are next converted to 1/3 octave band basis in the post-processing mode. All models and both measurements are compared in Figure 4 from 50 to 1600 Hz bands. Results of *Model A2* are relatively closer to the measurements and they yield almost the same resonant peaks as seen in the I_m measurement. The reason is that *Model A2* carries the same phase information as the I_s measurements, via the mutual impedance terms. Thus, *Model A2* incorporates the "acoustic short cuts" between neighboring anti-phase radiators. It is also observed that the mutual resistance is as important as the self-resistance in our analysis (when the Helmholtz number ky_i is less than 0.4, where y_i is the distance from the top surface of the plate). Further, the mutual reactance in the near field ($0 \le ka_i \le 1$) is found to be less important than the mutual resistance. The boundary element methods (*Models C1 and C2*) yield almost the same W spectrum. Overall, the boundary element methods suggest possible errors committed by the two-microphone method when carried out in a non-ideal acoustic environment, while also confirming that sufficient number of segments (meshes) is used in discrete analytical models.

Table 2: Comparison of sound power values obtained via experimental and analytical methods at the resonant frequencies of the plate.

Sound Power (dB re 1 pW) at Dominant Resonances						
Method (Measured or Predicted)	Plate Resonant Frequency (Hz)					
	276	420	688	920	1232	1504
Measured by I_m	71.7	64.7	66.5	73.3	76.5	70.4
Measured by I_s	65.0	77.3	79.1	68.5	75.2	78.2
Predicted by *Model A1* (Piston Radiator without mutual interaction)	78.3	77.4	78.4	86.7	85.9	79.9
Predicted by *Model A2* (Piston radiator with mutual interaction)	68.6	64.0	65.3	71.5	74.0	69.2
Predicted by *Model B* (Pulsating sphere)	87.1	86.2	86.4	95.0	93.1	87.2
Predicted by *Model C1* (Indirect BEM)	74.0	71.1	76.1	84.2	90.8	84.3
Predicted by *Model C2* (I_m simulated using BEM)	74.8	71.6	76.0	84.0	91.0	84.0

Note that the predictions of *Model C1* are closer to the spectrum obtained via the I_m measurement below 350 Hz. In the higher frequency range, measurements are closer to *Model A1* results or even to the pulsating sphere formulation (*Model B*). This suggests that boundary element formulation uses single-layered monopole type sources in the higher frequency range. Next we discuss the reasons for discrepancies between measurements themselves and between experimental and predicted sound powers. First, intensity measurements are made in near field where the acoustic field is mostly reactive. Consequently, intensities are very low at or near the anti-resonant frequencies even though the sound pressures remain high. Thus, the acoustic intensity spectrum exhibits sharper anti-resonances. Pressure-intensity index spectrum for each measurement reveals that up to 20 dB values are seen at the lower frequencies (below $350 Hz$) where rigid body motions are dominant. This might be the reason for relatively large differences between models and experiments in the lower frequency region. Second, recall that the frequency response functions (and intensities) from 36 different regions are spatially averaged to give the total power spectra. The frequency response functions contribute more to surface vibration measurements than the sound related measurements. Thus, in some regions, measured spectra have serious discrepancies. These might be corrected to some extent by using more discrete segments (discrete sources) on the plate.

In the intensity method, finite difference errors could be significant when the microphone separation distance is approximately equal to the distance of the measurement location (y) from the source[22]. Here, in this study, they are almost equal ($\Delta y = 18\ mm$, and $y = 17\ mm$), which would pose the finite difference approximation error as a dominant source of error. Experimentally, the plate is attached to a stinger via a bolted connection where the nut and a small portion of the stinger extend above the top surface of the plate. Thus, near field measurements corresponding to the segment in the middle of the plate are not exactly achieved at the mid-point of this partition. Moreover, the bolted connection itself would disturb the near field radiation field. As this particular segment is expected to be one of the most efficient radiation regions of the plate, measurements might have been underestimated because of above mentioned reasons. For the surface intensity measurements, a miniature accelerometer is attached on the discrete partitions in the middle of each partition and a microphone is placed in

its close proximity. Besides, accelerometer might have disturbed the sound field contaminating the information captured by the microphone, while causing some mass loading at higher frequencies. Further, there is a phasing problem in this measurement technique as one sensor gathers data from a dispersive wave medium where the other one from a non-dispersive wave medium.

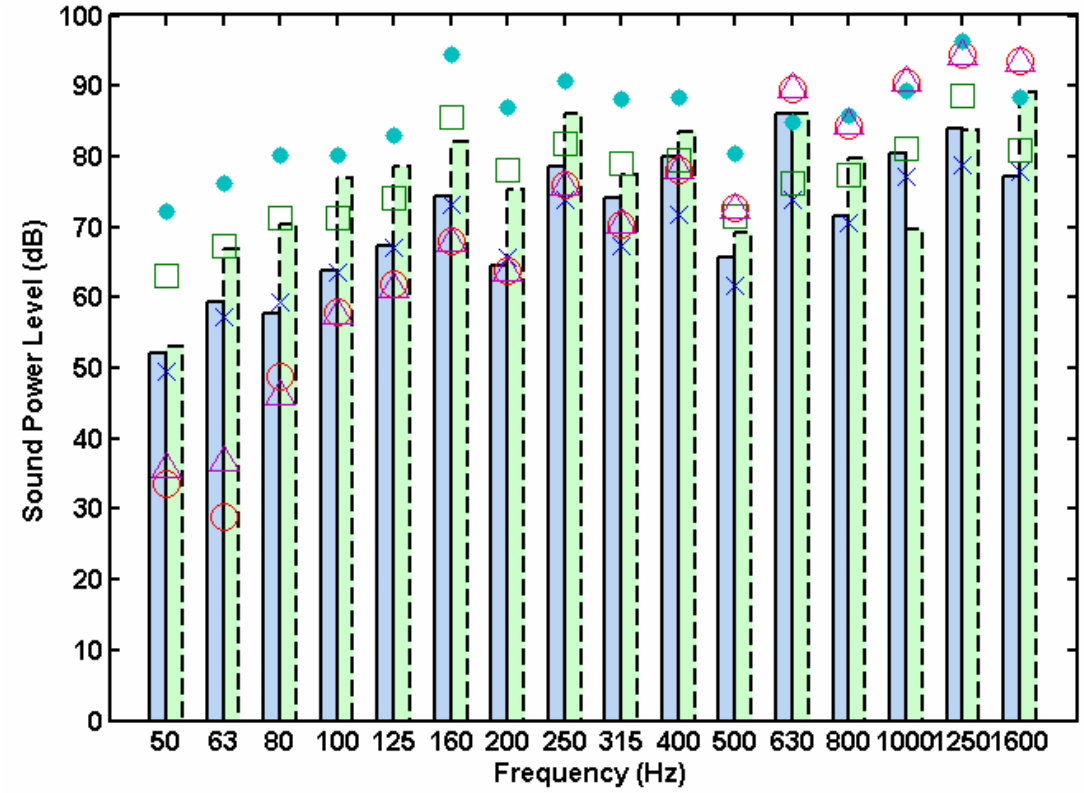

Figure 4: Comparison of measured (given by bars) and predicted (given by discrete symbols) sound powers W , dB re 1.0 pW on 1/3 octave band basis. Key: Green bars (- - -): measured by the surface intensity (I_s) method; blue bars (——): measured by the two-microphone acoustic intensity (I_m) method; green open squares: predicted by *Model A1*; blue crosses: predicted by *Model A2*; blue solid circles: predicted by *Model B*; red open circles: predicted by *Model C1*; red open triangles: predicted by *Model C2*.

The near field acoustic intensity measurements are carried out only on the top of the plate. However, our computational study (based on the BEM, *Model C1*) indicates that the other sides might be important as well. Results are reported in Figure 5. For instance, the edges contribute to the overall radiation more than we had presumed in the lower frequency range. Also, cancellations are seen at low frequencies when the radiation from the top plate is examined. That suggests the importance of measurements from sides as well as from the bottom of the plate which are not made.

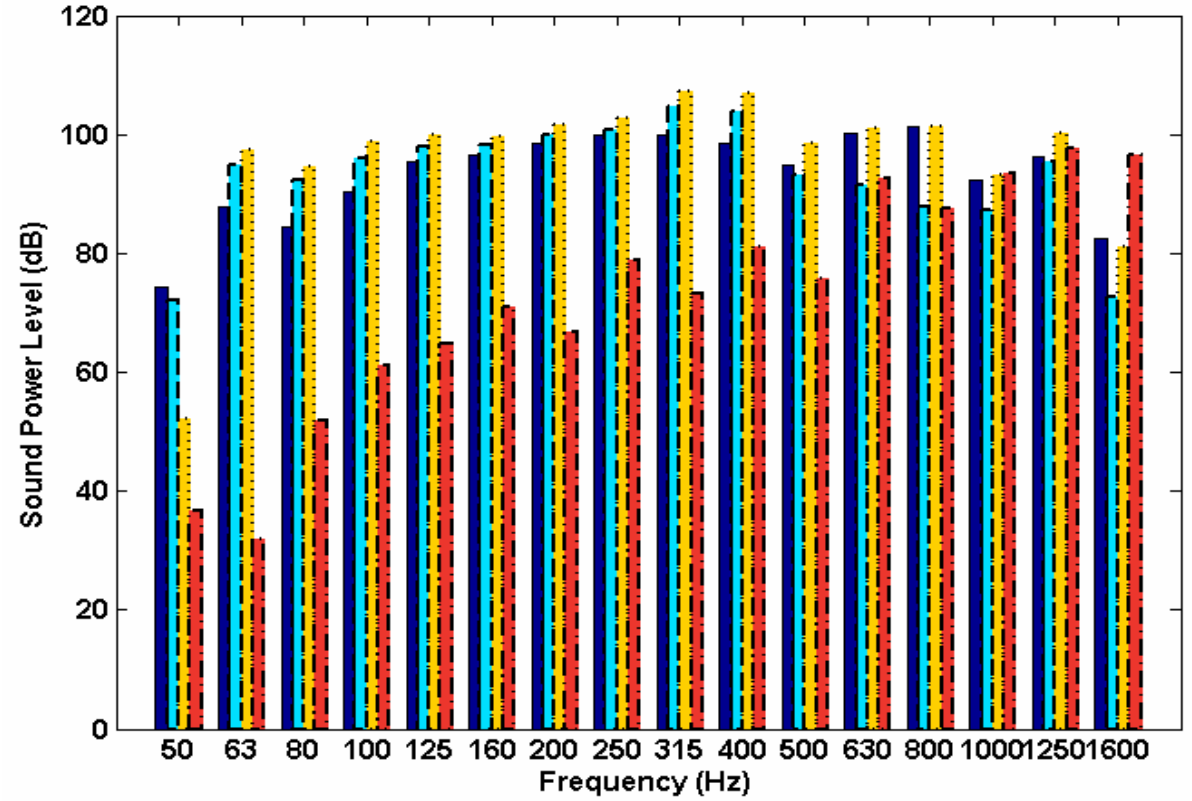

Figure 5: Contribution of sound powers W , dB re 1.0 pW, from different regions of the plate on 1/3 octave band basis. Key: Dark blue bars (——): from the plate center; light blue bars (- - -): from the plate corners; yellow bars (-.-.-): from the plate edges (including the corners), red bars (. . .): from the top surface of the plate.

7. CONCLUSION

Three analytical formulations (*A1, A2 and B*) used in our study are assumed to be discretized sources radiating in an infinite baffle. Note that the discrete models carry the phase information obtained via vibration measurements. However, baffled conditions are not achieved especially for the segments at the edges and corners. Further, *Models A1 and B* assume that as the sources radiate into a half-sphere independent from each other, e.g. without any acoustic interaction. Such discrete radiators are based on the premise that they convert all mechanical (vibratory) energy in to the sound mode. Moreover, these discrete sources do not carry any directivity information as they radiate equally in the radial direction within a hemi-spherical radiation surface. Nonetheless, results of the piston radiator formulation with mutual impedances (*Model A2*) are relatively closer to the surface intensity measurements. The boundary element method (*C1 and C2*) predicts only the acoustic field and thus its predictions are similar to acoustic intensity measurements at least over the lower frequency range. Even though predictions and measurements do not perfectly match, this paper clearly demonstrates that the mutual radiation resistance terms (in the near field of a vibrating free-free plate) are as important as the self-radiation resistance terms. For instance, *Model A1* and *Model B* overestimate the sound power (and radiation efficiency) spectra. Consequently, one should utilize both analytical and computational (boundary element) models to investigate the near field acoustics. A higher dimensional analytical or hybrid model might be efficient though more vibration measurements would be needed. Finally, we encourage researchers to examine the near fields of typical plate radiators with emphasis on resonant vibrations and share their analytical and experimental

results. Collective efforts would lead to some benchmark solutions that are needed by the practitioners.

ACKNOWLEDGEMENTS

The authors wish to thank Dr. Rajendra Gunda of the Ansol Inc., Hilliard Ohio for providing access to the BEM software *Coustyx*[20] and for technical discussions.

REFERENCES

[1] F. J. Fahy and P. Gardonio, *Sound and Structural Vibration: Radiation, Transmission and Response* (Academic Press, London, 2007).

[2] N. Atalla and J. Nicolas, "A new tool for predicting rapidly and rigorously the radiation efficiency of plate-like structures," *J. Acoust. Soc. Am.,* **95**(6), 3369-3378 (1994).

[3] M. F. Jacobsen, R. Singh, and F. B. Oswald, "Acoustic Efficiency Models of a Simple Gearbox," *Army Research Laboratory Technical Report,* ARL-TR-1111 (1996).

[4] W. L. Lee and H. J. Gibeling, "Determination of the mutual radiation resistances of a rectangular plate and their impact on the radiated sound power," *J. Sound Vib*., **229**(5), 1213-1233 (2000).

[5] T. Takahagi, M. Nakai and Y. Tamai, "Near field sound radiation from simply supported rectangular plates," *J. Sound Vib*., **185**(3), 455-4713 (1995).

[6] F. Cervera, H. Estelles, F. Galvez, and F. Belmar, "Sound intensity in the near field above a vibrating flat plate," *Noise Cont. Eng. J.,* **45** (5), 193-199 (1997).

[7] L. Shuyu, "Study on the radiation acoustic field of rectangular radiators in flexural vibration," *J. Sound Vib*., **254**(3), 469-479 (2002).

[8] D. J. Gorman, "Free Vibration Analysis of Completely Free Rectangular Plates by the Superposition-Galerkin Method," *J. Sound Vib*., **237**(5), 901-914 (2000).

[9] D. J. Gorman, "Free In-plane Vibration Analysis of Rectangular Plates by the Method of Superposition," *J. Sound Vib*., **272**, 831-851 (2004).

[10] L. Shuyu, "Study on the Flexural Vibration of Rectangular Thin Plates with Free Boundary Conditions," *J. Sound Vib*., **239**(5), 1063-1071 (2001).

[11] J. B. Fahnline and G. H. Koopmann, "A lumped parameter model for the acoustic power output from a vibrating structure," *J. Acoust. Soc. Am*., **100**(6) 3539-3547 (1996).

[12] J. B. Fahnline and G. H. Koopmann, "Numerical implementation of the lumped parameter model for the acoustic power output of a vibrating structure," *J. Acoust. Soc. Am*., **102**(1) 179-192 (1997).

[13] N. Hashimoto, "Measurement of sound radiation efficiency by the discrete calculation method," *App. Acoust*., **62** 429-446 (2001).

[14] G. Zhen, W. Zhongzhang and G. Tun, "Relation between plate vibration and its sound field," *Noise Cont. Eng. J.*, **32** (1), 35-41 (1989).

[15] G. H. Koopmann and J.B. Fahnline, *Designing Quiet Structures* (Academic Press, California, 1997).

[16] P. M. Morse and K. U. Ingard, *Theoretical Acoustics* (Princeton University Press, Princeton, New Jersey, 1987).

[17] J. W. S. Rayleigh, *The Theory of Sound: Volume 2* (Dover Publishers Inc., New York, 1945).

[18] R. M. Aarts, A. J. E. M. Janssen, Approximation of the Struve function H1 occurring in impedance calculations," *J. Acoust. Soc. Am*., **113**(5) 2635-2637 (2003).

[19] F.J. Fahy, "Measurement of acoustic intensity using the cross-spectral density of two microphone signals," *J. Acoust. Soc. Am*., **62**(4) 1057-1059 (1977).

[20] R. Gunda, *Coustyx Analytical Manual* (Ansol Inc., Hilliard, Ohio, USA, 2007).

[21] R. Gunda, S. Vijayakar, Acoustic radiation from an automotive gearbox, *SAE Noise and Vibration Conference Proceedings*, Paper No: 2007-01-2170, (2007).

[22] G. Steyer, "Spectral Methods for the Estimation of Acoustic Intensity, Energy Density, and Surface Velocity using a Multimicrophone Probe," *Ph.D Thesis,* The Ohio State University (1984).